

Theory of complex-coordinate transformation acoustics for non-Hermitian metamaterials

Hao-Xiang Li(李澔翔), Yang Tan(谭杨), Jing Yang(杨京), and Bin Liang(梁彬)
Citation: Chin. Phys. B, 2023, 32 (**9**): 094301. DOI: 10.1088/1674-1056/acc3fc
Journal homepage: http://cpb.iphy.ac.cn; http://iopscience.iop.org/cpb

What follows is a list of articles you may be interested in

Characteristic analysis of scattering field in two-layer media by Green's function

Ping Zhang(张萍), Zhi-Ying Liu(刘智颖), Shou-Guo Yan(阎守国), Juan Huang(黄娟), and Bi-Xing Zhang(张碧星)
Chin. Phys. B, 2023, 32 (**6**): 064301. DOI: 10.1088/1674-1056/aca3a0

Reconfigurable source illusion device for airborne sound using an enclosed adjustable piezoelectric metasurface

Yi-Fan Tang(唐一璠) and Shu-Yu Lin(林书玉)
Chin. Phys. B, 2023, 32 (**3**): 034306. DOI: 10.1088/1674-1056/ac9fc0

Effect of porous surface layer on wave propagation in elastic cylinder immersed in fluid

Na-Na Su(苏娜娜), Qing-Bang Han(韩庆邦), Ming-Lei Shan(单鸣雷), and Cheng Yin(殷澄)
Chin. Phys. B, 2023, 32 (**1**): 014301. DOI: 10.1088/1674-1056/ac6ee6

One-dimensional $\mathcal{PT}$-symmetric acoustic heterostructure

Hai-Xiao Zhang(张海啸), Wei Xiong(熊威), Ying Cheng(程营), and Xiao-Jun Liu(刘晓峻)
Chin. Phys. B, 2022, 31 (**12**): 124301. DOI: 10.1088/1674-1056/ac90b3

Controlling acoustic orbital angular momentum with artificial structures: From physics to application

Wei Wang(王未), Jingjing Liu(刘京京), Bin Liang (梁彬), and Jianchun Cheng(程建春)
Chin. Phys. B, 2022, 31 (**9**): 094302. DOI: 10.1088/1674-1056/ac7868

Theory of complex-coordinate transformation acoustics for non-Hermitian metamaterials

Hao-Xiang Li(李澔翔), Yang Tan(谭杨), Jing Yang(杨京), and Bin Liang(梁彬)†

Collaborative Innovation Center of Advanced Microstructures and Key Laboratory of Modern Acoustics, MOE, Institute of Acoustics, Department of Physics, Nanjing University, Nanjing 210093, *China*

(Received 26 January 2023; revised manuscript received 5 March 2023; accepted manuscript online 14 March 2023)

Transformation acoustics (TA) has emerged as a powerful tool for designing several intriguing conceptual devices, which can manipulate acoustic waves in a flexible manner, yet their applications are limited in Hermitian materials. In this work, we propose the theory of complex-coordinate transformation acoustics (CCTA) and verify the effectiveness in realizing acoustic non-Hermitian metamaterials. Especially, we apply this theory for the first time to the design of acoustic parity–time ($\mathcal{PT}$) and antisymmetric parity–time ($\mathcal{APT}$) metamaterials and demonstrate two distinctive examples. First, we use this method to obtain the exceptional points (EPs) of the $\mathcal{PT}/\mathcal{APT}$ system and observe the spontaneous phase transition of the scattering matrix in the transformation parameter space. Second, by selecting the Jacobian matrix's constitutive parameters, the $\mathcal{PT}/\mathcal{APT}$-symmetric system can also be configured to approach the zero and pole of the scattering matrix, behaving as an acoustic coherent perfect absorber and equivalent laser. We envision our proposed CCTA-based paradigm to open the way for exploring the non-Hermitian physics and finding application in the design of acoustic functional devices such as absorbers and amplifiers whose material parameters are hard to realize by using the conventional transformation method.

Keywords: complex-coordinate transformation acoustics, acoustic non-Hermitian metamaterials, exceptional points, acoustic coherent perfect absorber and equivalent laser

PACS: 43.20.+g, 43.28.+h, 43.35.+d, 43.38.+n **DOI:** 10.1088/1674-1056/acc3fc

1. Introduction

Transformation acoustics, which is developed from transformation optics[1–5] and direct current conductivity equations,[6] has been studied extensively in the past decade. By establishing a correspondence between material parameters and coordinate transformations, transformation acoustics provides an effective method for designing new acoustic devices.[7–9] One of the most famous and intriguing devices is the invisibility cloak,[10–18] which is able to eliminate reflected sound waves but inevitably results in inhomogeneous and anisotropic parameters inside the cloaking shell. In order to solve the problem that the signals from the outside environment cannot reach the interior of the cloaked domain, a cloaking mechanism has been proposed, which maps the cloaked object to main body of the host material and the cloaking shell only consists of complementary medium made of a single-negative material, so that the parameters are independent of the host material and communication with the outside world is allowed.[19] Despite the fact that transformation acoustics with real mapping functions has proven effective in steering the trajectory of acoustic waves, it still cannot manipulate the field amplitude in prescribed ways, limiting its applications for designing non-Hermitian devices with complex material parameters in nonconservative systems.

Non-Hermitian physics can be verified by using acoustics and electromagnetics, which not only provide a better understanding[20–22] but also bring non-Hermitian physics closer to practical applications.[23,24] Several interesting researches have shown unique features of exceptional point and exceptional ring[25,26] and the extraordinary capabilities in manipulating wavefronts asymmetrically.[27–29] Recent explorations of loss and gain within the framework of non-Hermitian systems play important roles in controlling acoustic transport, especially amplitude modulation.[8,30–33] In non-Hermitian physics, $\mathcal{PT}$-symmetric system with complex refractive index profile $n(-\boldsymbol{r}) = n^*(\boldsymbol{r})$ is an intriguing branch, whose Hamiltonian commutes with the $\mathcal{PT}$ operator, demonstrating remarkable physical properties.[34–46] Recently, as another striking property of non-Hermitian systems, $\mathcal{APT}$ symmetry has been proved, defined by $\{\mathcal{PT}, H\} = 0$, which may facilitate the experiments since it requires either gain or loss.[47–49] With the help of the positive and negative refractive index materials, many intriguing effects can beachieved, such as chiral mode transfer,[50] quantum squeezing and sensing,[51] and shift of EPs.[52] However, the artificial modulation of the imaginary part of wave vector in non-conservative systems, which is crucial for the amplification and attenuation of acoustic waves and the design of non-Hermitian acoustic metamaterials, would require the transformation acoustic method to adapt to complex spatial coordinate space and map complex coordinates.

Here we show that the theoretical framework of transformation acoustics can be extended through the use of complex mapping functions. We derive the theory of complex-coordinate transformation acoustics, and demonstrate how the transformation acoustics is directly related to engineering of

†Corresponding author. E-mail: liangbin@nju.edu.cn

© 2023 Chinese Physical Society and IOP Publishing Ltd

non-Hermitian medium, which provides additional degree of freedom to modulate the amplitude and propagation direction of sound waves simultaneously. To the best of our knowledge, no complex-coordinate transformation has been explored in acoustic systems. Specifically, by artificially designing the constitutive parameters of the transfer matrix, we derive the relation between the transmitted and reflected waves and realize the flexible control of EPs in the one-dimensional layered $\mathcal{PT}/\mathcal{APT}$-symmetric structure and investigate the phase transition process in the parameter space. We can also observe the coherent perfect absorber (CPA) and lasing mode in the $\mathcal{PT}/\mathcal{APT}$ metamaterials when modulating the constitutive parameters of the Jacobian matrix. A non-Hermitian material can be constructed by using our theory, extending the scope of application for transformation acoustics. Furthermore, it can reduce the complexity of material parameters in comparison with traditional realcoordinate transformation, which may inspire the experimental implementation of a perfect cloak which has not been realized before.[33,50]

2. Jacobian matrix for $\mathcal{PT}$ and $\mathcal{APT}$ symmetries

Now, we start from the acoustic wave equation with Cartesian coordinates $\boldsymbol{r} = (x, y, z)$ in the time harmonic form

$$\nabla \cdot \left[\underline{\underline{\rho}}(\boldsymbol{r})^{-1} \nabla p(\boldsymbol{r})\right] = -\frac{\omega^2}{\kappa(\boldsymbol{r})} p(\boldsymbol{r}), \tag{1}$$

where ρ is the density tensor, κ is the bulk modulus, and ω is the angular frequency. Analogously to the invariance of the conductivity equation, we map each point in the original space to another space based on a coordinate transformation with $p[\boldsymbol{r}'(\boldsymbol{r})] = p(\boldsymbol{r})$. The acoustic equation in the new space becomes

$$\nabla' \cdot \left[\underline{\underline{\rho}}'(\boldsymbol{r}')^{-1} \nabla' p'(\boldsymbol{r}')\right] = -\frac{\omega^2}{\kappa'(\boldsymbol{r}')} p'(\boldsymbol{r}'), \tag{2}$$

where

$$\begin{aligned} \underline{\underline{\rho}}'(\boldsymbol{r}')^{-1} &= \frac{\underline{\underline{J}}(\boldsymbol{r})[\underline{\underline{\rho}}(\boldsymbol{r})^{-1}]\underline{\underline{J}}(\boldsymbol{r})^{\mathrm{T}}}{\det \underline{\underline{J}}(\boldsymbol{r})}, \\ \kappa'(\boldsymbol{r}') &= \kappa(\boldsymbol{r}) \det \underline{\underline{J}}(\boldsymbol{r}), \end{aligned} \tag{3}$$

In Eq. (3), $\underline{\underline{J}} = \partial(x', y', z')/\partial(x, y, z)$ indicates the Jacobian matrix of the transformation, and the symbol det and the superscripts -1 and T denote the determinant, the inverse, and the transpose, respectively. It is worth mentioning that in contrast to the traditional coordinate transformation, the coordinates of the original real space can be mapped into complex values, which provides an effective strategy to manipulate the amplitude of acoustic waves. As an important example of non-Hermitian physics, here we focus on the acoustic systems under $\mathcal{PT}$ and $\mathcal{APT}$ symmetries.

In order to make the refractive index satisfy the $\mathcal{PT}$-symmetry conditions $n(\boldsymbol{r}) = n^*(-\boldsymbol{r})$, the material parameters need to satisfy $\underline{\underline{\rho}}(-\boldsymbol{r}) = \underline{\underline{\rho}}^*(\boldsymbol{r})$, $\kappa(-\boldsymbol{r}) = \kappa^*(\boldsymbol{r})$ (see Eq. (B3) in Appendix B for the commutation of the $\mathcal{PT}$ and pseudo-Hamiltonian operators). Such conditions are automatically met if the Jacobian matrix is chosen as

$$\underline{\underline{J}}(-\boldsymbol{r}) = \underline{\underline{J}}^*(\boldsymbol{r}), \tag{4}$$

where the transformed material in the complex coordinate system is assumed to be homogeneous and anisotropic. As for the $\mathcal{APT}$-symmetry conditions $\underline{\underline{\rho}}(-\boldsymbol{r}) = -\underline{\underline{\rho}}^*(\boldsymbol{r})$, $\kappa(-\boldsymbol{r}) = -\kappa^*(\boldsymbol{r})$,[53] the Jacobian matrix needs to satisfy

$$\underline{\underline{J}}(-\boldsymbol{r}) = -\underline{\underline{J}}^*(\boldsymbol{r}), \tag{5}$$

which has been proved theoretically in Appendix C. As a result of our proposed theoretical framework of CCTA, by combining Eqs. (3)–(5), we can generate systematic $\mathcal{PT}$ and $\mathcal{APT}$ metamaterials and explain their acoustic properties in terms of analytically continued complex coordinates in the auxiliary free space. For simplicity but without loss of generality, here we consider a one-dimensional (1D) scenario illustrated in Fig. 1, which features a slab-type configuration placed in air ($\rho_0 = 1.21$ kg/m^3, $\kappa_0 = 1.42 \times 10^5$ Pa), corresponding to the coordinate transformation

$$x' = xu(x), \quad y' = yv(x), \quad z' = zw(x), \quad |x| \le d, \tag{6}$$

with the identity transformation implicitly assumed for $|x| > d$ (i.e. outside the slab region), d is the thickness of the loss and gain medium, which is set to 2λ.

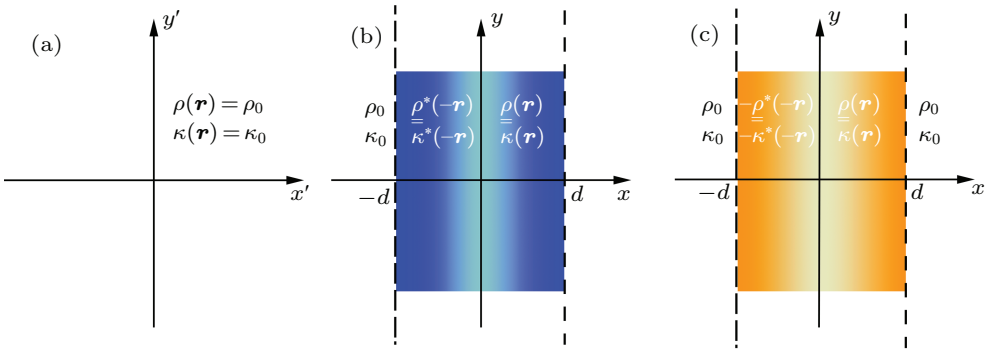


Fig. 1. Schematic diagram of (a) free space, (b) 1D acoustic $\mathcal{PT}$-symmetric structure, and (c) 1D acoustic $\mathcal{APT}$-symmetric structure of thickness $2d$.

3. Derivation of scattering matrix

We first use the CCTA method to derive the scattering matrix S of the 1D $\mathcal{PT}$-symmetric structure in Fig. 1(b). The corresponding Jacobian matrix can be written as

$$\underline{\underline{J}}(\boldsymbol{r}) = \begin{bmatrix} \frac{\partial x'}{\partial x} & \frac{\partial x'}{\partial y} & \frac{\partial x'}{\partial z} \\ \frac{\partial y'}{\partial x} & \frac{\partial y'}{\partial y} & \frac{\partial y'}{\partial z} \\ \frac{\partial z'}{\partial x} & \frac{\partial z'}{\partial y} & \frac{\partial z'}{\partial z} \end{bmatrix} = \begin{bmatrix} u(x)+\dot{u}(x)x & 0 & 0 \\ \dot{v}(x)y & v(x) & 0 \\ \dot{w}(x)z & 0 & w(x) \end{bmatrix}, \tag{7}$$

with the overdot denoting differentiation with respect to the argument. The $\mathcal{PT}$-symmetry condition requires

$$u(-x) = u^*(x), \quad v(-x) = v^*(x), \quad w(-x) = w^*(x), \tag{8}$$

which has been proved theoretically in Appendix C. For simplicity, here we consider a coordinate transformation of discontinuous functions

$$\begin{aligned} &u(x) = u_0^*, \quad v(x) = v_0^*, \quad w(x) = w_0^*, \quad -d \le x \le 0, \\ &u(x) = u_0, \quad v(x) = v_0, \quad w(x) = w_0, \quad 0 \le x \le d, \end{aligned} \tag{9}$$

which yields a $\mathcal{PT}$-metamaterial slab. As plane harmonic acoustic waves propagate upon $\mathcal{PT}$-symmetric structures, the background pressure field (p) can be expressed as

$$p(x) = \begin{cases} A\mathrm{e}^{-\mathrm{i}k_0(x+d)} + B\mathrm{e}^{\mathrm{i}k_0(x+d)}, & x < -d, \\ C\mathrm{e}^{-\mathrm{i}k_0(x-d)} + D\mathrm{e}^{\mathrm{i}k_0(x-d)}, & x > d, \end{cases} \tag{10}$$

where k_0 is the wave number for the background medium, A, B, C, and D are the amplitudes of the forward and backward propagating waves in the left and the right background mediums, respectively. The time-harmonic $[\exp(\mathrm{i}\omega t)]$ is omitted here for convenience. According to it, we use a transfer matrix to describe the relation between the acoustic waves in the left background medium and right background medium as

$$\begin{bmatrix} C \\ D \end{bmatrix} = M \begin{bmatrix} A \\ B \end{bmatrix}. \tag{11}$$

By enforcing

$$u_0 = \alpha + \mathrm{i}\beta, \quad v_0 w_0 = u_0, \tag{12}$$

the transfer matrix $M_{\mathcal{PT}}$ can be deduced, which is shown in Appendix D. When $D = 0$ or $A = 0$ is imposed on the boundary condition for single left or right incidence, the complex transmission (t_{L} or t_{R}) and reflection (r_{L} or r_{R}) coefficients of the $\mathcal{PT}$-symmetric structure can be expressed in terms of the components of the transfer matrix $M_{\mathcal{PT}}$ as follows:

$$\begin{aligned} t_{\mathrm{L}} = t_{\mathrm{R}} = t &= \frac{1}{M_{2,2}} = \frac{2(\alpha^2+\beta^2)}{2\beta^2\cosh\delta + \alpha[2\alpha\cos\gamma + \mathrm{i}(1+\alpha^2+\beta^2)\sin\gamma] - \mathrm{i}\beta(-1+\alpha^2+\beta^2)\sinh\delta}, \\ r_{\mathrm{L}} &= -\frac{M_{2,1}}{M_{2,2}} = -\frac{\mathrm{i}[2\alpha\beta(-\cos\gamma+\cosh\delta) + \alpha(-1+\alpha^2+\beta^2)\sin\gamma - \beta(1+\alpha^2+\beta^2)\sinh\delta]}{2\beta^2\cosh\delta + \alpha[2\alpha\cos\gamma + \mathrm{i}(1+\alpha^2+\beta^2)\sin\gamma] - \mathrm{i}\beta(-1+\alpha^2+\beta^2)\sinh\delta}, \\ r_{\mathrm{R}} &= \frac{M_{1,2}}{M_{2,2}} = \frac{\mathrm{i}\{-\alpha[2\beta\cos\gamma - 2\beta\cosh\delta + (-1+\alpha^2+\beta^2)\sin\gamma] + \beta(1+\alpha^2+\beta^2)\sinh\delta\}}{2\beta^2\cosh\delta + \alpha[2\alpha\cos\gamma + \mathrm{i}(1+\alpha^2+\beta^2)\sin\gamma] - \mathrm{i}\beta(-1+\alpha^2+\beta^2)\sinh\delta}, \end{aligned} \tag{13}$$

where $\gamma = 2\alpha k_0 d$ and $\delta = 2\beta k_0 d$. And the scattering matrix can be written as

$$\begin{bmatrix} C \\ B \end{bmatrix} = S \begin{bmatrix} A \\ D \end{bmatrix}, \quad S = \begin{bmatrix} t & r_{\mathrm{R}} \\ r_{\mathrm{L}} & t \end{bmatrix}. \tag{14}$$

It is not difficult to find that the transmission coefficient and reflection coefficient satisfy the relation (see Appendix D for the derivation of transfer matrix)

$$r_{\mathrm{L}} r_{\mathrm{R}}^* = 1 - |t|^2, \tag{15}$$

which is the generalized energy-conservation relation in the $\mathcal{PT}$-symmetric structure.[6]

Furthermore, by changing the form of the Jacobian matrix as follows:

$$u(-x) = -u^*(x), \quad v(-x) = -v^*(x), \quad w(-x) = -w^*(x), \tag{16}$$

we can achieve the requirement in Eq. (5) and realize the $\mathcal{APT}$ metamaterials. The transmission coefficient and reflection coefficient of the $\mathcal{APT}$ symmetric structure can be deduced and expressed as (see Appendix D for the derivation of transfer matrix $M_{\mathcal{APT}}$)

$$\begin{aligned} t_{\mathrm{L}} = t_{\mathrm{R}} = t &= \frac{1}{M_{2,2}} = \frac{4(\alpha^2+\beta^2)}{4\beta^2\cos\gamma - 2\beta(\alpha^2+\beta^2-1)\sin\gamma + \alpha(-\alpha^2-\beta^2+2\alpha-1)\mathrm{e}^{\delta} + \alpha(\alpha^2+\beta^2+2\alpha+1)\mathrm{e}^{-\delta}}, \\ r_{\mathrm{L}} &= -\frac{M_{2,1}}{M_{2,2}} = -\frac{4\mathrm{i}\alpha\beta\cos\gamma - 2\beta(\alpha^2+\beta^2+1)\sin\gamma + \alpha(-\alpha^2-\beta^2-2\mathrm{i}\beta+1)\mathrm{e}^{\delta} + \alpha(\alpha^2+\beta^2-2\mathrm{i}\beta-1)\mathrm{e}^{-\delta}}{4\beta^2\cos\gamma - 2\beta(\alpha^2+\beta^2-1)\sin\gamma + \alpha(-\alpha^2-\beta^2+2\alpha-1)\mathrm{e}^{\delta} + \alpha(\alpha^2+\beta^2+2\alpha+1)\mathrm{e}^{-\delta}}, \\ r_{\mathrm{R}} &= \frac{M_{1,2}}{M_{2,2}} = \frac{4\mathrm{i}\alpha\beta\cos\gamma - 2\beta(-\alpha^2-\beta^2-1)\sin\gamma + \alpha(\alpha^2+\beta^2-2\mathrm{i}\beta-1)\mathrm{e}^{\delta} + \alpha(-\alpha^2-\beta^2-2\mathrm{i}\beta+1)\mathrm{e}^{-\delta}}{4\beta^2\cos\gamma - 2\beta(\alpha^2+\beta^2-1)\sin\gamma + \alpha(-\alpha^2-\beta^2+2\alpha-1)\mathrm{e}^{\delta} + \alpha(\alpha^2+\beta^2+2\alpha+1)\mathrm{e}^{-\delta}}, \end{aligned} \tag{17}$$

where $\gamma = 2\alpha k_0 d$ and $\delta = 2\beta k_0 d$. It is not difficult to find the relation between the elementary components $\mathrm{Im}(t) = 0$, and $r_\mathrm{L} = r_\mathrm{R}^*$ demonstrating that our proposed method can be utilized to realize the acoustic $\mathcal{APT}$ metamaterials, whose concept has been extended to acoustics recently.[53]

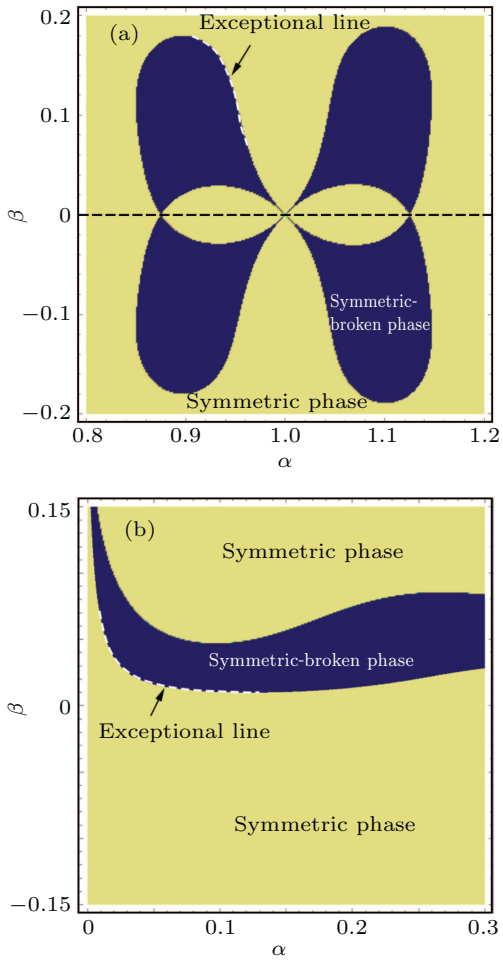


Fig. 2. Phase diagram of scattering matrix of (a) 1D $\mathcal{PT}$-symmetric structure and (b) 1D $\mathcal{APT}$-symmetric structure, with yellow (blue) region corresponding to the symmetric scattering phase (symmetry-broken phase), and boundaries between the two regions indicating phase transition marked by white dashed line.

In order to describe the relation between the scattering phase and transformation parameters, we further investigate the phase transition process of the scattering matrix of the 1D $\mathcal{PT}/\mathcal{APT}$-symmetric structures in the α–β parameter space, as shown in Figs. 2(a) and 2(b). The yellow region corresponds to the symmetric scattering phase, while the blue region corresponds to the symmetry-broken phase. The boundaries between the two regions indicate the phase transition. By changing the value of α and β, the constitutive parameters of Jacobian matrix can be further modulated, showing the phase transition point (EP), at which some unique scattering characteristics such as asymmetric reflection can be observed. Furthermore, we can find that the phase diagram of the scattering matrix in the $\mathcal{PT}$-symmetric structure is symmetric with respect to $\beta = 0$, which originates from the conjugate symmetric relation between the loss and gain. While in the $\mathcal{APT}$-symmetric structure, the symmetric-broken phase is sandwiched between two symmetric phases, which means that the scattering matrix can undergo two phase transmissions if we increase the value of β with a fixed α.

4. Applications

4.1. Modulation of EPs in metamaterial slab via CCTA method

Here we demonstrate theoretically that EPs in the $\mathcal{PT}$ and $\mathcal{APT}$ symmetric systems, which result in a spontaneous phase transition from symmetric phase to symmetry-broken phase, both can be formed at an arbitrary frequency in our designed slab via the CCTA method. To demonstrate the unidirectional reflection at the EPs, we first consider an isotropic $\mathcal{PT}$-metamaterial slab with a thickness of $d = 2\lambda$, excited by a plane wave. As an example, we set the operation frequency $f_0 = 3430$ Hz, and enforce $u_0 = v_0 w_0 = \alpha + \mathrm{i}\beta = 0.951 + 0.115\mathrm{i}$ and $w_0 = 1$. Hence the density tensor and bulk modulus can be written as

$$\begin{aligned}
\underline{\underline{\rho}}(-d \le x \le 0) &= \begin{bmatrix} \rho_0 & 0 & 0 \\ 0 & \rho_0 & 0 \\ 0 & 0 & (1.06+0.26\mathrm{i})\rho_0 \end{bmatrix} \\
&= \underline{\underline{\rho}}^*(0 \le x \le d), \\
\kappa(-d \le x \le 0) &= \frac{\kappa_0}{0.89-0.22\mathrm{i}} = \left(\frac{\kappa_0}{0.89+0.22\mathrm{i}}\right)^* \\
&= \kappa^*(0 \le x \le d).
\end{aligned} \tag{18}$$

Figures 3(a) and 3(b) show the pressure amplitude distribution of the $\mathcal{PT}$-symmetric structure for incidence from the left and the right, showing the total transmission ($|t| \approx 1$) and notable difference between the responses to incidence from the left (reflection $|r_\mathrm{L}|$ is almost 0) and the right ($|r_\mathrm{R}| = 2.071$). We also depict the absolute value of eigenvalues $|\lambda_\pm|$ and the eigenvectors $\Psi_\pm$ given by $\left(1 \pm \sqrt{(r_\mathrm{L}/r_\mathrm{R})}\right)^\mathrm{T}$, as shown in Figs. 3(c) and 3(d). As $f > 3430$ Hz, the eigenvalues are unimodular and the eigenvectors are real, indicating that the system is in the $\mathcal{PT}$-symmetric phase. While $f < 3430$ Hz the $\mathcal{PT}$ operation transforms one eigenvector into the other, i.e., $\mathcal{PT}\Psi_\pm \propto \Psi_\mp$, suggesting that the system is in the $\mathcal{PT}$-broken phase. The spontaneous phase transition occurs at EP $f = 3430$ Hz, when the absolute values of the eigenvalues meet and bifurcate, as shown by dark dot.

The observation of EPs in the $\mathcal{APT}$-symmetric medium is also plotted in Figs. 4(a)–4(d). The two eigenvalues and eigenvectors can be written as[54]

$$\begin{aligned}
\lambda_\pm &= \mathrm{Re}(r_\mathrm{L}) \pm \sqrt{t^2 - \mathrm{Im}^2(r_\mathrm{L})}, \\
\Psi_\pm &= \begin{bmatrix} \Psi_1 \\ \Psi_2 \end{bmatrix} = \begin{bmatrix} 1 \\ \left(-\mathrm{i}\,\mathrm{Im}(r_\mathrm{L}) \pm \sqrt{t^2 - \mathrm{Im}^2(r_\mathrm{L})}\right)/t \end{bmatrix}.
\end{aligned} \tag{19}$$

When $t > \mathrm{Im}(r_\mathrm{L})$, the two eigenvalues $\lambda_\pm$ are both real and the absolute value of the second component of the eigenvectors

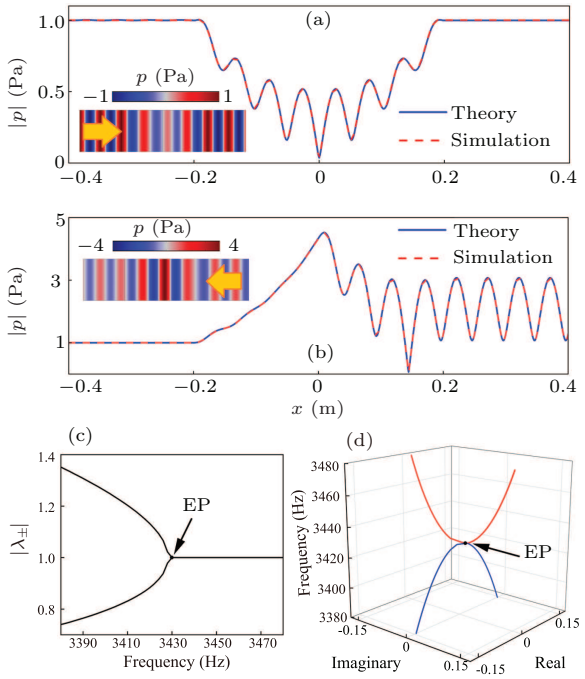


Fig. 3. EPs in $\mathcal{PT}$-symmetric structure, showing simulated pressure amplitude distributions of the $\mathcal{PT}$-symmetric structure under (a) the left incidence and (b) the right incidence with constitutive parameters $u_0 = v_0 w_0 = \alpha + \mathrm{i}\beta = 0.951 + 0.115\mathrm{i}$ and $w_0 = 1$, with inset showing pressure field distributions, and absolute values of (c) eigenvalues and (d) the second component of eigenvector of corresponding scattering matrix $\sqrt{r_\mathrm{L}/r_\mathrm{R}}$ for this acoustic $\mathcal{PT}$-symmetric medium, with eigenvectors normalized such that the first component is always unity.

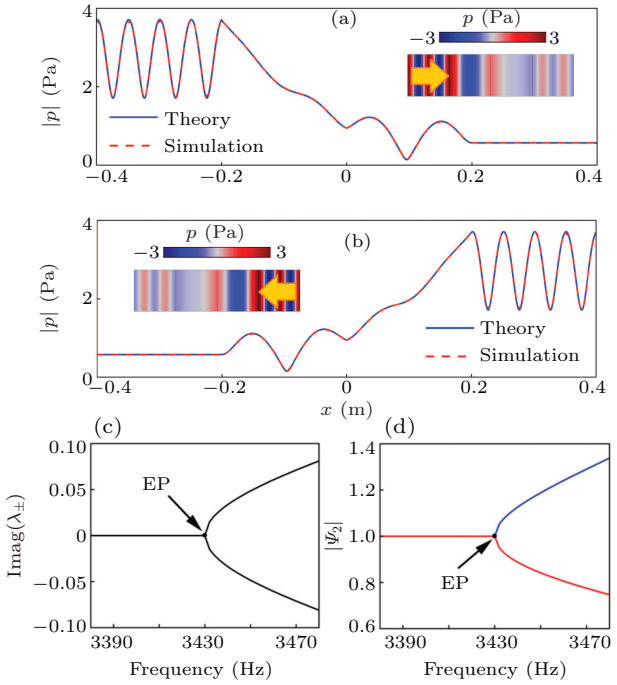


Fig. 4. EPs in $\mathcal{APT}$-symmetric structure, showing simulated pressure amplitude distributions of the $\mathcal{APT}$-symmetric structure under (a) the left and (b) the right incidence with constitutive parameters $u_0 = v_0 w_0 = \alpha + \mathrm{i}\beta = 0.458 + 0.095\mathrm{i}$ and $w_0 = 1$, with insets showing pressure field distributions, and (c) imaginary part of the eigenvalues and (d) absolute value of the second component of the eigenvectors for this $\mathcal{APT}$-symmetric medium, with eigenvectors normalized such that the first component is always unity.

$|\Psi_2|$ is 1, which corresponds to the $\mathcal{APT}$-symmetric phase. The other phase, where the two eigenvalues are conjugated, is referred to as the $\mathcal{APT}$-broken phase. In the simulation, by selecting appropriate constitutive parameters one has $t = \mathrm{Im}(r_\mathrm{L})$, which is referred to as an EP, and a spontaneous phase transition occurs, for both the eigenvalues and eigenvectors of the scattering matrix can be observed at 3430 Hz (see Appendix E for the asymmetric reflection in the $\mathcal{APT}$-symmetric structure).

4.2. CPA and laser effect via CCTA method

A 1D $\mathcal{PT}$-symmetric structure can act as a CPA and threshold laser simultaneously. In the following, we use the CCTA approach to realize this distinctive property by selecting the u, v, and w values in Eq. (9).

In an acoustic CPA-lasing mode, the elementary components of the transfer matrix need to satisfy

$$M_{1,1} = M_{2,2} = 0, \tag{20}$$

which means a zero and a pole of the S matrix coincide at a real frequency simultaneously.[46,55,56] Considering $t = 1/M_{2,2} \gg 1$, the system is in the $\mathcal{PT}$-broken phase,[33] whose eigenvalues s_a and s_b are nonunimodular and $s_\mathrm{a} s_\mathrm{b}^* = 1$. When two counter propagating coherent waves are incident in the form of two eigenstates, one with an eigenvalue ($s_\mathrm{a} = 0$) will be fully absorbed, indicating a CPA, while the other ($s_\mathrm{b} = 1/s_\mathrm{a} = \infty$) will make the acoustic system emit outgoing amplified waves, indicating threshold lasing.[57]

We simulate an example to achieve CPA-lasing mode by setting $d = 2\lambda = 0.2$ m, $f_0 = 3430$ Hz, $\alpha = 1.328$, and $\beta = 0.159$ (i.e., $v_0 w_0 = u_0 = 1.328 - 0.159\mathrm{i}$ and $w_0 = 1$), which enables a zero and a pole of the S matrix to coincide at 3430 Hz, as shown in Fig. 5(c). Here we use the output coefficient as a key parameter (Θ) for defining the ratio of total outgoing acoustic intensity to the total incoming intensity[58]

$$\Theta = \left(\frac{O_\mathrm{L} + O_\mathrm{R}}{I_\mathrm{L} + I_\mathrm{R}} \right), \tag{21}$$

where I_L, I_R, O_L, and O_R represent the input intensity and the output intensity on each side of the structure, respectively. By adjusting the phase offset between two incident waves to $-\pi/2$, a sharp absorption dip of Θ down to -37 dB can be observed near the operation frequency 3430 Hz (blue dotted line), which corresponds to the perfect absorption of sound waves (Fig. 5(a)). Meanwhile, with the phase offset switched to $\pi/2$, it is the lasing mode that the power flows are completely reversed and the amplitudes of the outgoing waves are found to be nearly 180 times that of the incident waves (Fig. 5(b)), with a maximum amplified Θ of 45 dB near the

same wavelength (red dotted line). We search for the conditions that Θ reaches minimum and maximum, which indicates that the output signal is completely absorbed and significantly amplified, corresponding to the CPA and lasing mode. The contrast ratio Q between the Θ under two incident conditions can be expressed as[59]

$$Q = \frac{\Theta_{\max}}{\Theta_{\min}}, \tag{22}$$

which shows that the highest intensity contrast peak appears at 3430 Hz (black solid line) in Fig. 5(c).

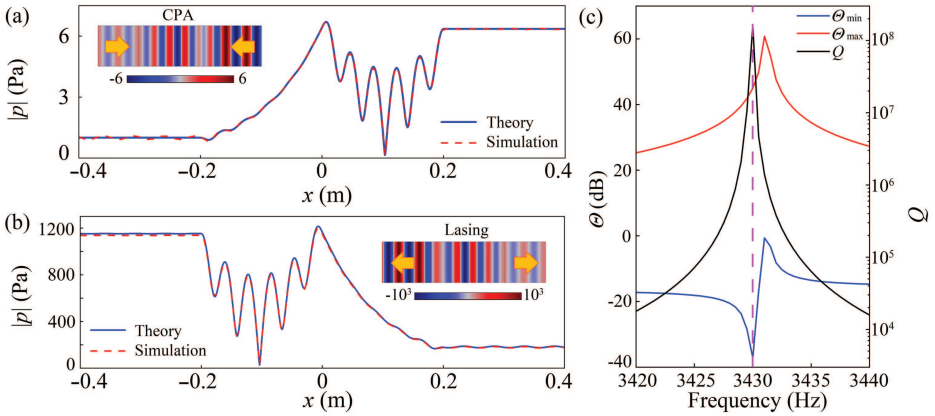


Fig. 5. Acoustic CPA-lasing mode achieved in $\mathcal{PT}$-symmetric structure via CCTA method, showing pressure amplitude distribution of structure in (a) CPA mode, (b) lasing mode under incidence of two-port coherent waves with the relation $D = (\mp 6.352\mathrm{i})A$, with inserts showing simulated pressure field distributions, with parameters being $d = 0.2$ m, $f_0 = 3430$ Hz, $\alpha = 1.328$, and $\beta = 0.159$, and (c) spectrum output coefficient $\Theta = (O_{\mathrm{L}} + O_{\mathrm{R}})/(I_{\mathrm{L}} + I_{\mathrm{R}})$ of the CPA-laser at frequency ranging from 3420 Hz to 3440 Hz, with blue, red, and black lines representing the output coefficient of CPA, laser, and the contrast ratio between maximum value and minimum value, respectively.

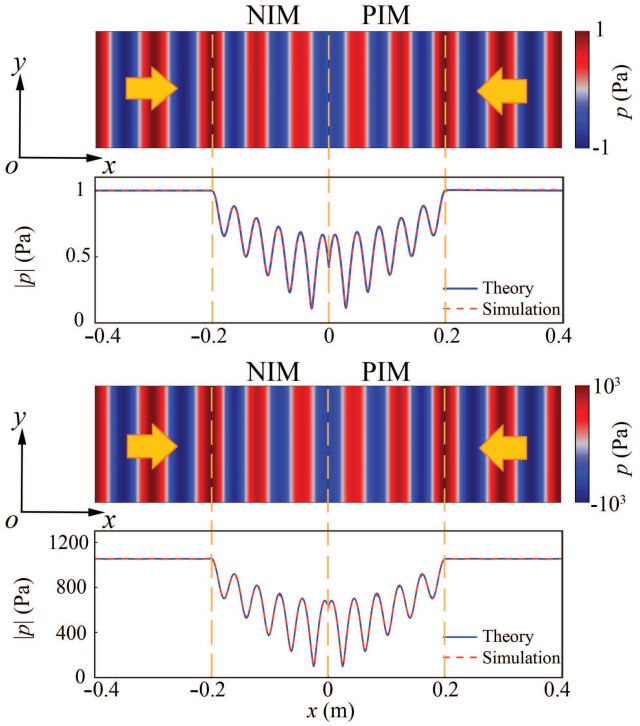


Fig. 6. (a) Acoustic CPA mode and (b) lasing mode achieved in $\mathcal{APT}$-symmetric structure via our proposed CCTA method, with simulated pressure field distributions (upper panels) and pressure amplitude distributions (lower panels) of the structure, under the incidence of two-port coherent waves with the constitutive parameters: $u_0 = 1.328 - 0.075\mathrm{i}$ and $u_0 = v_0 w_0 = 1.296 + 0.078\mathrm{i}$, demonstrating the CPA and lasing effect where two incident waves are significantly absorbed and amplified, and vertical dashed lines referring to the boundaries between the NIM, PIM, and background medium.

Moreover, the CCTA method we proposed in this work can also realize the CPA and laser mode in the $\mathcal{APT}$ metamaterials. In an acoustic CPA mode, the two outgoing waves will disappear, i.e., $A = D = 0$. Based on Eq. (11), the condition of achieving CPA can be written as

$$M_{1,1} = 0, \quad D = M_{2,1}A. \tag{23}$$

We demonstrate a typical example of the CPA effect and plot the simulated results in Fig. 6(a). With $d = 0.2$ m, $f = 3430$ Hz, the condition $M_{1,1} = 0$ can be achieved by choosing the constitutive parameters as $u_0 = v_0 w_0 = 1.328 - 0.075\mathrm{i}$ and $w_0 = 1$. Therefore, in the simulation, the two incident waves will be completely absorbed if they conform to the relation: $D = (0.983 + 0.211\mathrm{i})A$. Meanwhile, we find that the spatial derivation of the pressure field changes abruptly at the boundaries of the positive index material (PIM) and negative index material (NIM) despite the pressure field being still continuous at the boundaries, owing to the opposite sign of the mass densities of the PIM and NIM. In addition, if

$$M_{2,2} = 0, \tag{24}$$

the transmission coefficient approaches infinity, corresponding to the lasing mode. In the simulation, we set $u_0 = 1.296 + 0.078\mathrm{i}$ to satisfy the relation in Eq. (24). Figure 6(b) reveals that sound waves are amplified 1000 times under two incident waves with amplitudes $A = D$.

5. Conclusions

In this work, we drive the theory of the complex-coordinate transformation acoustics and show that such a

method can be used to design non-Hermitian acoustic materials, such as $\mathcal{PT}$ -metamaterials, modulating both the phase and amplitude of the acoustic field. Moreover, we demonstrate this idea in the one-dimensional $\mathcal{APT}$-symmetric structure and observe the spontaneous phase transition of the scattering matrix in the transformation parameter space, which has not been discussed before. The first example demonstrates that the EPs can be modulated in the $\mathcal{APT}$-symmetric structure by modulating the Jacobian matrix's constitutive parameters. In addition, the poles and the zeros of the scattering matrix can also be obtained for $\mathcal{APT}$-symmetric system to act as both a coherent perfect absorber and a laser. This transformation theory provides another aspect for us to design acoustic functional devices, which is expected to explore more fascinating non-Hermitian phenomena such as asymmetric absorbing,[60,61] amplifying,[62] and sensing.[63]

Appendix A: Pseudo-Hamiltonian formulation

In order to derive the general relation of material parameters in the $\mathcal{PT}/\mathcal{APT}$ metamaterials, we refer to the optical systems and consider the time-harmonic, sourceless acoustic equation pertaining to an anisotropic and inhomogeneous background described by the density tensor $\underline{\underline{\rho}}(\boldsymbol{r})$, bulk modulus $\kappa(\boldsymbol{r})$ and time variation $[\exp(\mathrm{i}\omega t)]$

$$\begin{cases} \nabla p(\boldsymbol{r}) = -\mathrm{i}\omega \underline{\underline{\rho}}(\boldsymbol{r}) \cdot \boldsymbol{v}(\boldsymbol{r}), \\ \nabla \cdot \boldsymbol{v}(\boldsymbol{r}) = -\dfrac{\mathrm{i}\omega p(\boldsymbol{r})}{\kappa(\boldsymbol{r})}. \end{cases} \tag{A1}$$

Using a method similar to that in Ref. [45] we can convert Eq. (A1) into an eigenproblem in a compact operator form, specifically,

$$\underline{\underline{\mathcal{L}}} \cdot \begin{bmatrix} \underline{p} \\ \underline{v} \end{bmatrix} = \omega \begin{bmatrix} \underline{p} \\ \underline{v} \end{bmatrix}, \tag{A2}$$

with

$$\underline{p} = \begin{bmatrix} p \\ p \\ p \end{bmatrix}, \quad \underline{v} = \begin{bmatrix} v_x \\ v_y \\ v_z \end{bmatrix}, \tag{A3}$$

$$\underline{\underline{\mathcal{L}}} = \begin{bmatrix} \underline{\underline{0}} & \mathrm{i}\kappa(\boldsymbol{r}) \cdot \underline{\nabla}(\boldsymbol{r}) \\ \mathrm{i}\underline{\underline{\rho}}^{-1}(\boldsymbol{r}) \cdot \underline{\underline{\Omega}}(\boldsymbol{r}) & \underline{\underline{0}} \end{bmatrix}, \tag{A4}$$

where $\underline{\underline{0}}$ is the 3×3 null matrix, and

$$\kappa(\boldsymbol{r}) = \begin{bmatrix} \kappa \\ \kappa \\ \kappa \end{bmatrix}, \quad \nabla(\boldsymbol{r}) = \begin{bmatrix} \dfrac{\partial}{\partial x} \\ \dfrac{\partial}{\partial y} \\ \dfrac{\partial}{\partial z} \end{bmatrix}^{\mathrm{T}},$$

$$\underline{\underline{\Omega}}(\boldsymbol{r}) = \begin{bmatrix} \dfrac{\partial}{\partial x} & 0 & 0 \\ 0 & \dfrac{\partial}{\partial y} & 0 \\ 0 & 0 & \dfrac{\partial}{\partial z} \end{bmatrix}. \tag{A5}$$

Appendix B: Commutation of $\mathcal{PT}/\mathcal{APT}$ and pseudo-Hamiltonian operators

Since the system satisfies the $\mathcal{PT}$ symmetry condition and the operator $\underline{\underline{\mathcal{L}}}$ plays a role of a pseudo-Hamiltonian, i.e.,

$$\underline{\underline{\mathcal{L}}}\mathcal{PT} = \mathcal{PT}\underline{\underline{\mathcal{L}}}. \tag{B1}$$

We can achieve [recalling that $(\mathcal{PT})^2 = 1$]

$$\mathcal{PT}\underline{\underline{\mathcal{L}}}\mathcal{PT} = \underline{\underline{\mathcal{L}}}. \tag{B2}$$

Substituting Eq. (A4) into Eq. (B2) and considering the restraint condition: $\mathcal{PT}(\mathrm{i}\Omega) = \mathrm{i}\Omega$ and $\mathcal{PT}(\mathrm{i}\nabla) = \mathrm{i}\nabla$, the material parameters should satisfy

$$\underline{\underline{\rho}}(-\boldsymbol{r}) = \underline{\underline{\rho}}^*(\boldsymbol{r}), \quad \kappa(-\boldsymbol{r}) = \kappa^*(\boldsymbol{r}), \tag{B3}$$

which is the distribution condition of the refractive index under $\mathcal{PT}$ symmetry.[64]

And if the acoustic system is under the $\mathcal{APT}$-symmetry condition, i.e.,

$$\underline{\underline{\mathcal{L}}}\mathcal{PT} = -\mathcal{PT}\underline{\underline{\mathcal{L}}}, \tag{B4}$$

using the method similar to that for Eqs. (B2) and (B3), we can find the antisymmetric refractive index and mass density as follows:

$$\underline{\underline{\rho}}(-\boldsymbol{r}) = -\underline{\underline{\rho}}^*(\boldsymbol{r}), \quad \kappa(-\boldsymbol{r}) = -\kappa^*(\boldsymbol{r}). \tag{B5}$$

Referring to the literature related to acoustic $\mathcal{APT}$ symmetry,[64] we obtain the more generalized distribution characteristics of material parameters.

Appendix C: Relation among constitutive parameters for $\mathcal{PT}/\mathcal{APT}$ symmetry

We first derive the relation among constitutive parameters for the 1D $\mathcal{PT}$ metamaterial in Fig. 1(b). Substituting Eq. (7) into Eq. (3), we obtain the transformed material density and bulk modulus of elasticity, which are given below:

$$\underline{\underline{\rho}}(\boldsymbol{r})^{-1} = \left[\det \underline{\underline{J}}(\boldsymbol{r}) \underline{\underline{J}}^{-1}(\boldsymbol{r}) \underline{\underline{\rho_0}}(\boldsymbol{r})^{-1} \underline{\underline{J}}^{-T}(\boldsymbol{r})\right]$$

$$= a\begin{bmatrix} \dfrac{1}{\rho_0\left(u(x)+x\dot{u}(x)\right)^2} & -\dfrac{y\dot{v}(x)}{\rho_0 v(x)\left(u(x)+x\dot{u}(x)\right)^2} & -\dfrac{z\dot{w}(x)}{\rho_0 w(x)(u(x)+x\dot{u}(x))^2} \\ -\dfrac{y\dot{v}(x)}{\rho_0 v(x)(u(x)+x\dot{u}(x))^2} & \dfrac{(u(x)+x\dot{u}(x))^2+y^2\dot{v}^2(x)}{\rho_0 v^2(x)(u(x)+x\dot{u}(x))^2} & \dfrac{yzv(x)w(x)\dot{v}(x)\dot{w}(x)}{\rho_0(u(x)v(x)w(x)+xv(x)w(x)\dot{u}(x))^2} \\ -\dfrac{z\dot{w}(x)}{\rho_0 w(x)(u(x)+x\dot{u}(x))} & -\dfrac{yzv(x)w(x)\dot{v}(x)\dot{w}(x)}{\rho_0(u(x)v(x)w(x)+xv(x)w(x)\dot{u}(x))^2} & \dfrac{z^2\dot{w}^2(x)+(u(x)+x\dot{u}(x))^2}{\rho_0 w^2(x)(u(x)+x\dot{u}(x))^2} \end{bmatrix},$$

$$\kappa(\boldsymbol{r}) = \frac{\kappa_0}{a}, \tag{C1}$$

where

$$a = \det(J) = v(x)w(x)(u(x)+\dot{u}(x)x). \tag{C2}$$

Considering that the material parameters in the $\mathcal{PT}$-symmetric structure should satisfy the relation in Eq. (B3), the constitutive parameters are required to meet the following condition:

$$u(-x) = u^*(x),\ \ v(-x) = v^*(x),\ \ w(-x) = w^*(x)\,. \tag{C3}$$

As reported in the main text, if the constitutive parameters satisfy Eq. (C3), the corresponding Jacobian matrix will automatically fulfill the relation in Eq. (4). And since we consider a coordinate transformation of discontinuous functions expressed in Eq. (9), the Jacobian matrix and material parameters should satisfy the relation

$$\begin{aligned}
\underline{\underline{J}}(-d\le x\le 0) &= \begin{bmatrix} u_0^* & 0 & 0 \\ 0 & v_0^* & 0 \\ 0 & 0 & w_0^* \end{bmatrix} \\
&= \begin{bmatrix} u_0 & 0 & 0 \\ 0 & v_0 & 0 \\ 0 & 0 & w_0 \end{bmatrix}^* = \underline{\underline{J}}^*(0\le x\le d), \\
\underline{\underline{\rho}}(-d\le x\le 0) &= \begin{bmatrix} \dfrac{\rho_0 u_0^*}{v_0^* w_0^*} & 0 & 0 \\ 0 & \dfrac{\rho_0 v_0^*}{u_0^* w_0^*} & 0 \\ 0 & 0 & \dfrac{\rho_0 w_0^*}{u_0^* v_0^*} \end{bmatrix} \\
&= \begin{bmatrix} \dfrac{\rho_0 u_0}{v_0 w_0} & 0 & 0 \\ 0 & \dfrac{\rho_0 v_0}{u_0 w_0} & 0 \\ 0 & 0 & \dfrac{\rho_0 w_0}{u_0 v_0} \end{bmatrix}^* = \underline{\underline{\rho}}^*(0\le x\le d), \\
\kappa(-d\le x\le 0) &= \frac{\kappa_0}{u_0^* v_0^* w_0^*} = \left(\frac{\kappa_0}{u_0 v_0 w_0}\right)^* \\
&= \kappa^*(0\le x\le d),
\end{aligned} \tag{C4}$$

which clearly shows that the transformed material parameters satisfy the $\mathcal{PT}$-symmetry condition.

As for the $\mathcal{APT}$-symmetric structure in Fig. 1(c), we consider a coordinate transformation of discontinuous functions

$$\begin{aligned}
&u(x) = -u_0^*,\ v(x) = -v_0^*,\ w(x) = -w_0^*,\ -d\le x\le 0, \\
&u(x) = u_0,\quad v(x) = v_0,\quad w(x) = w_0,\quad 0\le x\le 0.
\end{aligned} \tag{C5}$$

And the relations of the Jacobian matrix and material parameters can be given by

$$\begin{aligned}
\underline{\underline{J}}(-d\le x\le 0) &= \begin{bmatrix} -u_0^* & 0 & 0 \\ 0 & -v_0^* & 0 \\ 0 & 0 & -w_0^* \end{bmatrix} \\
&= -\begin{bmatrix} u_0 & 0 & 0 \\ 0 & v_0 & 0 \\ 0 & 0 & w_0 \end{bmatrix}^* = -\underline{\underline{J}}^*(0\le x\le d), \\
\underline{\underline{\rho}}(-d\le x\le 0) &= \begin{bmatrix} -\dfrac{\rho_0 u_0^*}{v_0^* w_0^*} & 0 & 0 \\ 0 & -\dfrac{\rho_0 v_0^*}{u_0^* w_0^*} & 0 \\ 0 & 0 & -\dfrac{\rho_0 w_0^*}{u_0^* v_0^*} \end{bmatrix} \\
&= -\begin{bmatrix} \dfrac{\rho_0 u_0}{v_0 w_0} & 0 & 0 \\ 0 & \dfrac{\rho_0 v_0}{u_0 w_0} & 0 \\ 0 & 0 & \dfrac{\rho_0 w_0}{u_0 v_0} \end{bmatrix}^* \\
&= -\underline{\underline{\rho}}^*(0\le x\le d), \\
\kappa(-d\le x\le 0) &= -\frac{\kappa_0}{u_0^* v_0^* w_0^*} = -\left(\frac{\kappa_0}{u_0 v_0 w_0}\right)^* \\
&= -\kappa^*(0\le x\le d).
\end{aligned} \tag{C6}$$

Appendix D: Derivation of transfer matrix *M*

As shown in Fig. D1, a 1D acoustic $\mathcal{PT}$-symmetric structure consisting of two layers of media, is immersed in a background medium with a density of ρ_0 and a velocity of c_0. The total field within each medium be regarded as a superposition of forward and backward propagating wave. At the boundary $x=-d$, the pressure fields (p), which are on both sides of the boundary, can be written as

$$p(x) = \begin{cases} A\,\mathrm{e}^{-\mathrm{i}k_0(x+d)} + B\,\mathrm{e}^{\mathrm{i}k_0(x+d)}, & x<-d, \\ E\,\mathrm{e}^{-\mathrm{i}k_0(x+u_0^* d)} + F\,\mathrm{e}^{\mathrm{i}k_0(x+u_0^* d)}, & x>-d, \end{cases} \tag{D1}$$

where k_0 is the wave number for the background medium, A, B, E, and F are the amplitudes of the forward and backward propagating waves in the background and the loss medium, respectively.

Consider that the transformation relation between the sound pressure and vibration velocity at the boundary

satisfies[9]

$$p(x)=p'(x'),\quad v(x)=\frac{v'(x')\det(A)}{A},\tag{25}$$

where A is the Jacobian matrix of the transformation. We derive the transfer matrix at the boundary $x=-d$ as given below:

$$\begin{bmatrix}E\\F\end{bmatrix}=M_1\begin{bmatrix}A\\B\end{bmatrix},$$
$$M_1=\begin{bmatrix}\frac{1}{2}\left(1+\frac{1}{v_0^*w_0^*}\right) & \frac{1}{2}\left(1-\frac{1}{v_0^*w_0^*}\right)\\ \frac{1}{2}\left(1-\frac{1}{v_0^*w_0^*}\right) & \frac{1}{2}\left(1+\frac{1}{v_0^*w_0^*}\right)\end{bmatrix}.\tag{D3}$$

According to the Refs. [53,54,65], the transfer matrix on the left-hand side can be expressed as

$$T_1=\begin{bmatrix}\mathrm{e}^{-\mathrm{i}k_0u_0^*d} & 0\\ 0 & \mathrm{e}^{\mathrm{i}k_0u_0^*d}\end{bmatrix}.\tag{D4}$$

The transfer matrix $M=\begin{bmatrix}M_{1,1} & M_{1,2}\\ M_{2,1} & M_{2,2}\end{bmatrix}$ finally reads

$$\begin{aligned}M=&\frac{1}{8}\begin{bmatrix}1+v_0w_0 & 1-v_0w_0\\ 1-v_0w_0 & 1+v_0w_0\end{bmatrix}\begin{bmatrix}\mathrm{e}^{-\mathrm{i}k_0u_0d} & 0\\ 0 & \mathrm{e}^{\mathrm{i}k_0u_0d}\end{bmatrix}\\ &\times\begin{bmatrix}1+\frac{v_0w_0}{v_0^*w_0^*} & 1-\frac{v_0w_0}{v_0^*w_0^*}\\ 1-\frac{v_0w_0}{v_0^*w_0^*} & 1+\frac{v_0w_0}{v_0^*w_0^*}\end{bmatrix}\begin{bmatrix}\mathrm{e}^{-\mathrm{i}k_0u_0^*d} & 0\\ 0 & \mathrm{e}^{\mathrm{i}k_0u_0^*d}\end{bmatrix}\\ &\times\begin{bmatrix}1+\frac{1}{v_0^*w_0^*} & 1-\frac{1}{v_0^*w_0^*}\\ 1-\frac{1}{v_0^*w_0^*} & 1+\frac{1}{v_0^*w_0^*}\end{bmatrix}.\end{aligned}\tag{D5}$$

Let $u_0=\alpha+\mathrm{i}\beta$, and $v_0w_0=u_0$, then the four elementary components ($M_{1,1}$, $M_{1,2}$, $M_{2,1}$, and $M_{2,2}$) of the transfer matrix $M_{\mathcal{PT}}$ will be able to be simplified into the explicit expressions

$$\begin{aligned}M_{1,1}&=\frac{1}{2(\alpha^2+\beta^2)}\{2\beta^2\cosh\delta+\alpha[2\alpha\cos\gamma-\mathrm{i}(1+\alpha^2+\beta^2)\sin\gamma]+\mathrm{i}\beta(-1+\alpha^2+\beta^2)\sinh\delta\},\\ M_{1,2}&=\frac{\mathrm{i}}{2(\alpha^2+\beta^2)}\{-\alpha[2\beta\cos\gamma-2\beta\cosh\delta+(-1+\alpha^2+\beta^2)\sin\gamma]+\beta(1+\alpha^2+\beta^2)\sinh\delta\},\\ M_{2,1}&=\frac{\mathrm{i}}{2(\alpha^2+\beta^2)}[2\alpha\beta(-\cos\gamma+\cosh\delta)+\alpha(-1+\alpha^2+\beta^2)\sin\gamma-\beta(1+\alpha^2+\beta^2)\sinh\delta],\\ M_{2,2}&=\frac{1}{2(\alpha^2+\beta^2)}\{2\beta^2\cosh\delta+\alpha[2\alpha\cos\gamma+\mathrm{i}(1+\alpha^2+\beta^2)\sin\gamma]-\mathrm{i}\beta(-1+\alpha^2+\beta^2)\sinh\delta\},\end{aligned}\tag{D6}$$

where $\gamma=2\alpha k_0d$ and $\delta=2\beta k_0d$. By simplifying the formula above, we can find that the elementary components of the transfer matrix satisfy the relation $M_{2,2}=M_{1,1}^*$, $M_{1,2}=-M_{1,2}^*$, $M_{2,1}=-M_{2,1}^*$, which has been verified in the literature.[44,45,66]

As for the $\mathcal{APT}$-symmetric structure, the transfer matrix can be calculated in a similar way as the above-mentioned $\mathcal{PT}$-symmetric structure, while the difference is that considering the $\mathcal{APT}$-symmetry relationship (Eq. (C6)), a pair of positive index material (PIM) and negative index material (NIM) needs immersing in air. The transfer matrix $M_{\mathcal{APT}}$ can be written as

$$\begin{aligned}M=&\frac{1}{8}\begin{bmatrix}(1+v_0w_0) & (1-v_0w_0)\\ (1-v_0w_0) & (1+v_0w_0)\end{bmatrix}\begin{bmatrix}\mathrm{e}^{-\mathrm{i}k_0u_0d} & 0\\ 0 & \mathrm{e}^{\mathrm{i}k_0u_0d}\end{bmatrix}\\ &\times\begin{bmatrix}\left(1+\frac{v_0^*w_0^*}{v_0w_0}\right) & \left(1-\frac{v_0^*w_0^*}{v_0w_0}\right)\\ \left(1-\frac{v_0^*w_0^*}{v_0w_0}\right) & \left(1+\frac{v_0^*w_0^*}{v_0w_0}\right)\end{bmatrix}\begin{bmatrix}\mathrm{e}^{\mathrm{i}k_0u_0^*d} & 0\\ 0 & \mathrm{e}^{-\mathrm{i}k_0u_0^*d}\end{bmatrix}\\ &\times\begin{bmatrix}\left(1+\frac{1}{v_0^*w_0^*}\right) & \left(1-\frac{1}{v_0^*w_0^*}\right)\\ \left(1-\frac{1}{v_0^*w_0^*}\right) & \left(1+\frac{1}{v_0^*w_0^*}\right)\end{bmatrix}.\end{aligned}\tag{D7}$$

By setting $u_0=\alpha+\mathrm{i}\beta$, $v_0w_0=u_0$, the four elementary components ($M_{1,1}$, $M_{1,2}$, $M_{2,1}$, and $M_{2,2}$) can be simplified into

$$\begin{aligned}M_{1,1}&=\frac{1}{4(\alpha^2+\beta^2)}[4\beta^2\cos\gamma-2\beta(-\alpha^2-\beta^2+1)\sin\gamma+\alpha(\alpha^2+\beta^2+2\alpha+1)\mathrm{e}^{\delta}+\alpha(-\alpha^2-\beta^2+2\alpha-1)\mathrm{e}^{-\delta}],\\ M_{1,2}&=\frac{1}{4(\alpha^2+\beta^2)}[4\mathrm{i}\alpha\beta\cos\gamma-2\beta(-\alpha^2-\beta^2-1)\sin\gamma+\alpha(\alpha^2+\beta^2-2\mathrm{i}\beta-1)\mathrm{e}^{\delta}+\alpha(-\alpha^2-\beta^2-2\mathrm{i}\beta+1)\mathrm{e}^{-\delta}],\\ M_{2,1}&=\frac{1}{4(\alpha^2+\beta^2)}[4\mathrm{i}\alpha\beta\cos\gamma-2\beta(\alpha^2+\beta^2+1)\sin\gamma+\alpha(-\alpha^2-\beta^2-2\mathrm{i}\beta+1)\mathrm{e}^{\delta}+\alpha(\alpha^2+\beta^2-2\mathrm{i}\beta-1)\mathrm{e}^{-\delta}],\\ M_{2,2}&=\frac{1}{4(\alpha^2+\beta^2)}[4\beta^2\cos\gamma-2\beta(\alpha^2+\beta^2-1)\sin\gamma+\alpha(-\alpha^2-\beta^2+2\alpha-1)\mathrm{e}^{\delta}+\alpha(\alpha^2+\beta^2+2\alpha+1)\mathrm{e}^{-\delta}],\end{aligned}\tag{D8}$$

from which we can figure out the relation of the elementary components $\mathrm{Im}(M_{1,1})=\mathrm{Im}(M_{2,2})=0$ and $M_{1,2}=-M_{2,1}^*$ in the $\mathcal{APT}$-symmetric structures.

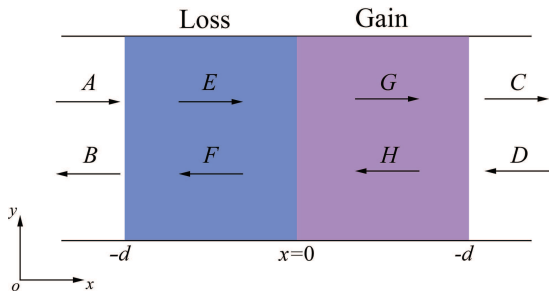


Fig. D1. Schematic diagram of 1D acoustic $\mathcal{PT}$-symmetric structure, consisting of a pair of loss and gain medium with the same width d immersed in a passive background medium (the leftmost and rightmost regions), with black lines indicating hard walls of structure.

Appendix E: Asymmetric reflection in $\mathcal{APT}$-symmetric structure

In the $\mathcal{APT}$-symmetric optical structure, the reflection coefficient and transmission coefficient satisfy the relation[53]

$$r_{\mathrm{L}} = r_{\mathrm{R}}^{*}, \quad \mathrm{Im}(t) = 0. \tag{E1}$$

According to Ref. [54], at the phase transition point, no particular property is found for the reflection coefficient and transmission coefficient, which makes it hard to judge whether the system is at the exact EP from Figs. 4(a) and 4(b). In order to further demonstrate this property, we depict the phase distribution at the upper boundary of the $\mathcal{APT}$-symmetric structure in Figs. E1(a) and E1(b), which shows a notable difference when the acoustic wave is incident from the left side and the right side, respectively. Furthermore, we calculate the reflection coefficient and transmission coefficient in Figs. 4(a) and 4(b) as given below:

$$t = -0.57, \quad r_{\mathrm{L}} = 2.65 - 0.57\mathrm{i}, \tag{E2}$$

which satisfy the relation $t = \pm\mathrm{Im}(r_{\mathrm{L}})$ at EPs, demonstrating that the $\mathcal{APT}$-symmetric structure can be modulated at the phase transition point by our complex-coordinate transformation method.

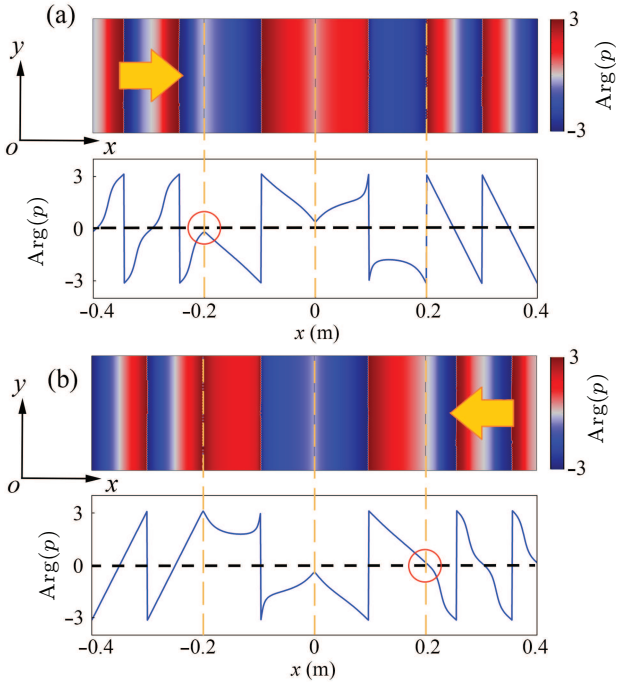


Fig. E1. Asymmetric reflection in $\mathcal{APT}$-symmetric structure. Simulated pressure field distributions (upper panels) and pressure amplitude distributions (lower panels) at the upper boundary of the $\mathcal{APT}$-symmetric structure under (a) left incidence and (b) right incidence, respectively, with constitutive parameters being $u_0 = v_0 w_0 = \alpha + \mathrm{i}\beta = 0.458 + 0.095\mathrm{i}$, and vertical dashed lines indicating boundaries between the NIM, PIM, and background medium.

Acknowledgements

Project supported by the National Key Research and Development Program of China (Grant No. 2022YFA1404402), the National Natural Science Foundation of China (Grant Nos. 12174190, 11634006, 12074286, and 81127901), the High-Performance Computing Center of Collaborative Innovation Center of Advanced Microstructures, and the the Priority Academic Program Development of Jiangsu Higher Education Institutions.

References

[1] Leonhardt U 2006 *Science* **312** 1777
[2] Pendry J B, Schurig D and Smith D R 2006 *Science* **312** 1780
[3] Leonhardt U and Philbin T G 2009 *Prog. Opt.* **53** 69
[4] Greenleaf A, Kurylev Y, Lassas M and Uhlmann G 2009 *Siam Review* **51** 3
[5] Chen H Y 2009 *J. Opt. A-Pure Appl. Opt.* **11** 075102
[6] Chen H Y and Chan C T 2010 *J. Phys. D* **43** 113001
[7] Cummer S A and Schurig D 2007 *New J. Phys.* **9** 45
[8] Chen H Y and Chan C T 2007 *Appl. Phys. Lett.* **91** 183518
[9] Cummer S A, Christensen J and Alu A 2016 *Nat. Rev. Mater.* **1** 16001
[10] Zhang S, Xia C G and Fang N 2011 *Phys. Rev. Lett.* **106** 024301
[11] Zigoneanu L, Popa B I and Cummer S A 2014 *Nat. Mater.* **13** 352
[12] Cummer S A, Popa B I, Schurig D, Smith D R, Pendry J, Rahm M and Starr A 2008 *Phys. Rev. Lett.* **100** 024301
[13] Torrent D and Sanchez-Dehesa J 2008 *New J. Phys.* **10** 063015
[14] Mei J, Ma G C, Yang M, Yang Z Y, Wen W J and Sheng P 2012 *Nat. Commun.* **3** 756
[15] Yang Z, Mei J, Yang M, Chan N H and Sheng P 2008 *Phys. Rev. Lett.* **101** 204301
[16] Ma G C and Sheng P 2016 *Sci. Adv.* **2** e1501595
[17] Liang Z X and Li J S 2012 *Phys. Rev. Lett.* **108** 114301
[18] Li J and Chan C T 2014 *Phys. Rev. E* **70** 055602
[19] Zhu X F, Liang B, Kan W W, Zou X Y and Cheng J C 2011 *Phys. Rev. Lett.* **106** 014301
[20] Tang W Y, Jiang X, Ding K, Xiao Y X, Zhang Z Q, Chan C T and Ma G C 2020 *Science* **370** 1077
[21] Achilleos V, Theocharis G, Richoux O and Pagneux V 2017 *Phys. Rev. B* **95** 144303
[22] Zhang L 2021 *Nat. Commun.* **12** 6297
[23] Ding K, Ma G C, Xiao M, Zhang Z Q and Chan C T 2016 *Phys. Rev. X* **6** 021007
[24] Noh J, Huang S, Chen K P and Rechtsman M C 2018 *Phys. Rev. Lett.* **120** 063902
[25] Wang B B, Ge Y, Yuan S Q, Jia D and Sun H X 2023 *Progress in Electromagnetics Research-Pier* **176** 1
[26] Wang B B, Jia D, Ge Y, Yuan S Q and Sun H X 2022 *New J. Phys.* **24** 113033
[27] Li Y, Shen C, Xie Y B, Li J F, Wang W Q, Cummer S A and Jing Y 2017 *Phys. Rev. Lett.* **119** 035501

[28] Wang X, Fang X S, Mao D X, Jing Y and Li Y 2019 *Phys. Rev. Lett.* **123** 214302
[29] Yang Y Z, Jia H, Bi Y F, Zhao H and Yang J 2019 *Phys. Rev. Appl.* **12** 034040
[30] El Ganainy R, Makris K G, Khajavikhan M, Musslimani Z H, Rotter S and Christodoulides D N 2018 *Nat. Phys.* **14** 11
[31] Ashida Y, Gong Z P and Ueda M 2020 *Adv. Phys.* **69** 249
[32] Gu Z M, Gao H, Cao P C, Liu T, Zhu X F and Zhu J 2021 *Phys. Rev. Appl.* **16** 057001
[33] Achilleos V, Theocharis G, Richoux O and Pagneux V 2017 *Phys. Rev. B* **95** 144303
[34] Konotop V V, Yang J K and Zezyulin D A 2016 *Rev. Mod. Phys.* **88** 035002
[35] Bender C M and Boettcher S 1998 *Phys. Rev. Lett.* **80** 5243
[36] Guo A, Salamo G J, Duchesne D, Morandotti R, Volatier Ravat M, Aimez V, Siviloglou G A and Christodoulides D N 2009 *Phys. Rev. Lett.* **103** 093902
[37] Zhu X F, Ramezani H, Shi C Z, Zhu J and Zhang X 2014 *Phys. Rev. X* **4** 031042
[38] Auregan Y and Pagneux V 2017 *Phys. Rev. Lett.* **118** 174301
[39] Ruter C E, Makris K G, Ganainy R E, Christodoulides D N, Segev M and Kip D 2010 *Nat. Phys.* **6** 192
[40] Chen P Y and Jung J 2016 *Phys. Rev. Appl.* **5** 064018
[41] Lin Z, Ramezani H, Eichelkraut T, Kottos T, Cao H and Christodoulides D N 2011 *Phys. Rev. Lett.* **106** 213901
[42] Li H X, Lopez M A, Zhu Y F, Fan X D, Torrent D, Liang B, Cheng J C and Christensen J 2019 *Research* **2019** 8345683
[43] Sounas D L, Fleury R and Alu A 2015 *Phys. Rev. Appl.* **4** 014005
[44] Longhi S 2010 *Phys. Rev. A* **82** 031801
[45] Chong Y D, Ge L and Stone A D 2011 *Phys. Rev. Lett.* **106** 093902
[46] Chong Y D, Ge L, Cao H and Stone A D 2010 *Phys. Rev. Lett.* **105** 053901
[47] Peng P, Cao W X, Shen C, Qu W Z, Wen J M, Jiang L and Xiao Y H 2016 *Nat. Phys.* **12** 1139
[48] Wu J H, Artoni M and La Rocca G C 2014 *Phys. Rev. Lett.* **113** 123004
[49] Antonosyan D A, Solntsev A S and Sukhorukov A A 2015 *Opt. Lett.* **40** 4575
[50] Geng L L, Zhang W X, Zhang X D and Zhou X M 2021 *P. Roy. Soc. A Mat.* **477** 20210641
[51] Luo X W, Zhang C W and Du S W 2022 *Phys. Rev. Lett.* **128** 173602
[52] Chen T Y, Xiao Z S, Jiang S, Li W X, Li J C, Wang Y F, Wang X C, Huang A P and Zhang H 2022 *J. Appl. Phys.* **131** 243101
[53] Ge L and Tureci H E 2013 *Phys. Rev. A* **88** 053810
[54] Hu T, Wei W, Zhu X F, Yao J and Wu D J 2021 *Phys. Rev. B* **104** 134110
[55] Longhi S and Feng L 2014 *Opt. Lett.* **39** 5026
[56] Huang C Y, Zhang R, Han J L, Zheng J and Xu J Q 2014 *Phys. Rev. A* **89** 023842
[57] Bai P, Ding K, Wang G, Luo J, Zhang Z Q, Chan C T, Wu Y and Lai Y 2016 *Phys. Rev. A* **94** 063841
[58] Wong Z J, Xu Y L, Kim J, Brien K, Wang Y, Feng L and Zhang X 2016 *Nat. Photon.* **10** 796
[59] Novitsky D V 2019 *J. Opt.* **21** 085101
[60] Long H Y, Cheng Y and Liu X J 2017 *Appl. Phys. Lett.* **111** 143502
[61] Li H X, Liang B and Cheng J C 2022 *Sci. Sin-Phys. Mech. As.* **52** 244302
[62] Jing H, Ozdemir S K, Lu X Y, Zhang J, Yang L and Nori F 2014 *Phys. Rev. Lett.* **113** 053604
[63] Sakhdari M, Farhat M and Chen P Y 2017 *New J. Phys.* **19** 065002
[64] Shi C Z, Dubois M, Chen Y, Cheng L, Ramezani H, Wang Y and Zhang X 2016 *Nat. Commun.* **7** 11110
[65] Fei Y, Liu Y W, Dong D X, Fan Y Q and Fu Y Y 2020 *Opt. Commun.* **474** 126123
[66] Ge L, Chong Y D and Stone A D 2012 *Phys. Rev. A* **85** 023802